

Combined deterministic-stochastic framework for modeling the agglomeration of colloidal particles

S. M. Mortuza, Lahiru K. Kariyawasam, and Soumik Banerjee*

School of Mechanical and Materials Engineering, Washington State University, Pullman, Washington 99164-2920, USA

(Received 17 March 2015; published 6 July 2015)

We present a multiscale model, based on molecular dynamics (MD) and kinetic Monte Carlo (kMC), to study the aggregation driven growth of colloidal particles. Coarse-grained molecular dynamics (CGMD) simulations are employed to detect key agglomeration events and calculate the corresponding rate constants. The kMC simulations employ these rate constants in a stochastic framework to track the growth of the agglomerates over longer time scales and length scales. One of the hallmarks of the model is a unique methodology to detect and characterize agglomeration events. The model accounts for individual cluster-scale effects such as change in size due to aggregation as well as local molecular-scale effects such as changes in the number of neighbors of each molecule in a colloidal cluster. Such definition of agglomeration events allows us to grow the cluster to sizes that are inaccessible to molecular simulations as well as track the shape of the growing cluster. A well-studied system, comprising fullerenes in NaCl electrolyte solution, was simulated to validate the model. Under the simulated conditions, the agglomeration process evolves from a diffusion limited cluster aggregation (DLCA) regime to percolating cluster in transition and finally to a gelation regime. Overall the data from the multiscale numerical model shows good agreement with existing theory of colloidal particle growth. Although in the present study we validated our model by specifically simulating fullerene agglomeration in electrolyte solution, the model is versatile and can be applied to a wide range of colloidal systems.

DOI: [10.1103/PhysRevE.92.013304](https://doi.org/10.1103/PhysRevE.92.013304)

PACS number(s): 02.70.-c, 61.43.Hv, 81.05.ub, 36.40.-c

I. INTRODUCTION

The dispersion and aggregation of colloidal particles such as gold, silver, iron, polystyrene, silica, and fullerene have substantial impacts on biological systems, engineering devices, and on the environment [1–16]. For instance, the preparation and delivery of drugs, solution-based fabrication of electronic devices, and purification of water through precipitation of colloidal impurities are greatly influenced by the stability and growth of colloidal particles in solutions. More specific examples of the applications of colloidal aggregation include the solution crystallization of pharmaceutical drugs and fabrication of thin film flexible electronic devices using solvent-based techniques [1–6,14–16]. The processing conditions for solvent-based fabrication, such as the choice of solvent medium and the concentration of colloidal particles, influence the growth mechanism of the particles and therefore their size distribution. In several of the above mentioned applications, controlled growth of the particles is necessary in order to attain optimum morphological structure of the aggregates. Hence, significant research efforts have been directed towards understanding agglomeration mechanisms in order to control the size and shape of resulting aggregates [1,2,17–25].

Both experimental and numerical techniques have been widely used to study the mechanisms of agglomeration of colloidal particles. These studies are in consensus that the interaction energy between colloidal particles plays an important role [22–31]. Typically, the relative magnitude of attractive van der Waals (VDW) and repulsive Coulombic forces between colloidal particles governs the agglomeration behavior of the particles [32,33]. Agglomeration occurs when the activation energy E_b , due to the long-range Coulombic repulsive interaction between approaching particles, can be

overcome. The likelihood that two particles will agglomerate and stick to each other is proportional to $e^{-(E_b/k_B T)}$, where k_B is Boltzmann's constant and T is the temperature of the system. If the long-range Coulombic repulsions are fully screened, $E_b \ll k_B T$, thus eliminating the energy barrier. Under such conditions, the short-range VDW attractions are dominant and lead to agglomeration. Due to the absence of the energy barrier, the agglomeration of the particles is completely governed by their diffusion resulting in a sticking probability of unity [32]. Such an agglomeration process is said to be diffusion limited cluster aggregation (DLCA), where particles diffuse randomly and stick together when they are in proximity and agglomerate spontaneously [17,18,20,21,34,35]. However, partial screening of electrostatic repulsion could lead to $E_b \gg k_B T$. Due to the presence of an energy barrier, the sticking probability of particles becomes less than unity [17,32]. Under such conditions, the agglomeration process, which is slower than DLCA, is referred to as reaction limited cluster aggregation (RLCA) [19,23,36,37]. Usually DLCA and RLCA processes are irreversible due to the presence of an attractive well [17,35]. However, relatively weak attractive forces and sufficiently high temperature increases the probability of the particles to escape from the attractive well and break up. Aggregation, under such conditions, is reversible and the particles restructure within the clusters or even dissociate from each other [17,30,38,39].

Both DLCA and RLCA mechanisms have been studied extensively for dilute systems, where the average distance between the clusters is greater than their size. However, nondilute conditions lead to increased connectivity of clusters that eventually form networks. In particular, the aggregation results in very compact gel-like structures [40–44] if the initial volume fraction of the colloidal particles is greater than ~ 0.05 [41,45]. Several studies have classified an intermediate process, referred to as percolation, during the formation of gels from solution. [40,46,47] The size and shape of agglomerates of colloidal particles resulting from the above

*Corresponding author: soumik.banerjee@wsu.edu

mentioned aggregation processes (DLCA, RLCA, percolation, and gelation) are well described by developing Monte Carlo based models of the corresponding processes, i.e., DLCA [17,18,20,21,34], RLCA [19,35,36], percolation [40,48,49], and gelation [46,50,51].

Due to their wide scale applications, the aggregation mechanism and size and shape of certain colloidal particles, such as gold, silver and silica, have been widely investigated using experiments and the above mentioned models [17,22–24,26–28,52]. In recent times, the aggregation behavior of fullerenes and its derivatives in solvents has generated significant scientific interests in myriad biological and environmental applications as well as in flexible electronic devices [1,2,10,11,53]. Specifically, solution-based processing to produce thin nanocomposite films of fullerene derivatives and conductive polymers is regarded as a cost-effective approach for manufacturing flexible electronic devices. For instance, organic photovoltaics (OPVs) employ photoactive layers comprising fullerene derivatives and polymers that are processed from a solution. The morphology of the solution-processed photoactive layers in OPVs is greatly influenced by the nature of agglomeration of fullerene derivatives in solvents [54–58]. On the other hand, the agglomeration mechanism of fullerene particles also determines the level of possible toxicological effects caused by unintended discharge of the particles in aquatic environments [1,3,10,11]. The aggregation of fullerenes and their derivatives therefore presents an interesting scientific problem in the realm of colloidal systems, with several important applications, and was therefore chosen as a model system in the present study.

Several studies have described agglomeration mechanism of fullerene particles in aquatic media relevant to environments and biological systems [1–3,11]. These studies have shown that the presence of salts promotes the agglomeration of fullerene and have predicted critical concentrations of the salts, at which a slow RLCA regime turns into a DLCA regime. However, the effect of concentration of fullerene on the critical salt concentrations and on the agglomeration process in aqueous media is still not understood well. Based on previous studies of fullerenes in organic solvents, where salts are typically not introduced, it is evident that increase in fullerene concentration enhances the aggregation rate of fullerenes [55,59–62]. Occasionally the aggregation happens so fast that the residence time of distinct fullerene particles is in the order of nanoseconds (ns). It is extremely difficult to capture such fast dynamics with experiments. The stochastic agglomeration models mentioned above cannot accurately predict the aggregation behavior of fullerene particles in a medium, since these models do not consider all relevant short range VDW and long-range Coulombic interactions among particles and the medium. Moreover, these stochastic agglomeration models are unable to track the evolution of the particles with respect to physical time.

On the other hand, molecular dynamics (MD), a deterministic technique, accounts for the intermolecular interactions and can be useful in studying the kinetics of fullerene agglomeration [63]. In OPV applications, MD has been widely used to study the morphology of solution-processed photoactive layers comprising fullerene derivatives, such as [6,6]-phenyl-C61-butyric acid methyl ester (PCBM) [61,62

64–67]. The objective of these studies was to determine the effect of processing conditions on the shape and size distribution of aggregates of fullerene derivatives and the resulting morphology of the photoactive layers. However, it is necessary to analyze large aggregates of the particles to predict the morphology of the photoactive layers at length scales relevant to OPVs. Obtaining large particle agglomerate structures of size in the order of 100 nm, the thickness of the photoactive layer, is not feasible using MD simulations. Hence, a reasonably comprehensive multiscale model needs to be developed and employed to investigate particle aggregation at large length scales, while accounting for long and short range atomistic interactions. The inherent limitations of previously reported experimental and numerical modeling based studies underscore the necessity of a comprehensive model, which can predict the size and shapes of the agglomerates at large length and time scales and determine the underlying mechanism for particle growth at various conditions.

In the current study we aim to combine MD, which can account for intermolecular interactions, with a stochastic technique, kinetic Monte Carlo (kMC), which can access the dynamics of particle agglomeration at large length and time scales. We demonstrate that the multiscale model can predict and characterize the evolution of size and shape of fullerene agglomerates from nano- to near micrometer length scales. The model can further provide a detailed description of the growth process at various conditions, such as the medium containing the fullerene particles and initial concentration of fullerene and salt or other chemical species present in the medium. In Sec. II we extensively describe the simulated systems, techniques, and assumptions we considered in developing the multiscale model. The results, obtained from the model, are validated with the currently available experimental and numerical studies and discussed in detail in Sec. III. It should be noted that fullerene has been chosen as a model system for the study. The model is, however, not limited to describing only fullerene agglomeration and can be used for a range of systems where agglomeration of small molecules is of importance.

II. METHODOLOGY

A. Theory: Kinetic Monte Carlo

In order to characterize the structure of fullerene agglomerates that range in size from 1 to 100 nm and understand the underlying growth mechanism in electrolyte solutions, we developed a new model that employs the kMC method. Particle growth in colloidal systems usually consists of a sequence of discrete transformations from one agglomerate size and shape to another, characteristic of a simple Markovian walk [68], where the evolution of the agglomerate state with time is governed by a master equation:

$$\frac{\partial P_A(t)}{\partial t} = - \sum_B W_{A \rightarrow B} P_A(t) + \sum_B W_{B \rightarrow A} P_B(t), \quad (1)$$

where A and B are successive states of the system, $P_A(t)$ is the probability that the system is in state A at time t , and $W_{A \rightarrow B}$ is the probability per unit time that the system will undergo a transition from state A to state B [69–72]. $W_{A \rightarrow B}$ is also called transition rate constant $k_{A \rightarrow B}$. The typical

number of states in models for cluster formation is so huge that an analytical solution of the corresponding high-dimensional master equation is not feasible. In contrast, a kMC algorithm helps to achieve a numerical solution to this master equation by generating an ensemble of trajectories, where each trajectory propagates the system correctly from state to state in the sense that the average over the entire ensemble of trajectories yields probability density functions $P_A(t)$ for all states A that fulfill the master equation [69–71]. The probability distribution function for the time of transition from state A to state B follows an exponential distribution:

$$P_{A \rightarrow B}(\Delta t) = k_{\text{total}} e^{-k_{\text{total}} \Delta t}, \quad (2)$$

where $k_{\text{total}} = \sum_{j=1}^E (k_{A-B})_j$ is the sum of the E possible transition rate constants. The probability of transition from state A to state B is proportional to its rate constant. Therefore, the executed process e (transition from $A \rightarrow B$) satisfies the following condition:

$$\sum_{j=1}^{e-1} (k_{A-B})_j < u_1 k_{\text{total}} \leq \sum_{j=1}^e (k_{A-B})_j, \quad (3)$$

where $u_1 \in (0, 1]$ is a uniform random number. For each transition event, a waiting time (Δt) is sampled using the following exponential distribution:

$$\Delta t = -\frac{\log u_2}{k_{\text{total}}}, \quad (4)$$

where $u_2 \in (0, 1]$ is a uniform random number.

Defining the events associated with individual agglomeration steps and finding the rate constants k_{A-B} of the events are necessary to develop a model that utilizes kMC technique to simulate fullerene agglomeration. The rate constants can be obtained from experiments, transition state theory, MD simulations, or other schemes [53,69,73–79]. In this work, k_{A-B} of all elementary processes related to the growth of fullerenes were calculated from coarse-grained molecular dynamics (CGMD) simulations of fullerene nanoparticles in electrolyte solutions. CGMD is a well-established method, which reduces the number of interacting sites in molecules to some beads instead of all the atoms, while maintaining the accuracy in the dynamics and structural properties desired from a simulation. Performing CGMD simulations in the current study allowed us to run simulations of larger domains, which significantly increased the number of events sampled for transitions from one cluster size and shape to another. The details of the computational models used for implementing CGMD and kMC are provided below.

B. Coarse-grained molecular dynamics simulations

In order to calculate rate constants of events related to the growth of fullerenes, we simulated systems comprising fullerenes in a monovalent (NaCl) electrolyte solution. We employed the Martini force field parameters for fullerenes, water, and NaCl [80–82]. Our simulated systems comprised of 1296 fullerene molecules, where each fullerene consisted of 16 beads (4:1 mapping), in 170 856 solvent beads, where each bead represents 4 water molecules. The corresponding mass fraction of fullerenes in the simulated systems was 7%. Na^+

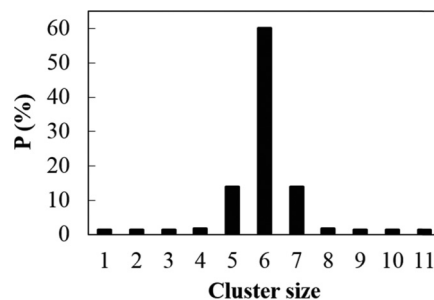


FIG. 1. The initial distribution of fullerene clusters modeled in CGMD simulations is shown. Here P represents the percentage of clusters of different sizes, defined by the number of fullerenes in a cluster.

and Cl^- ions were added to the solution and the numbers were varied from 162 to 5184 to simulate electrolyte concentrations from 0.01 to 0.4 M. In the Martini force field, each bead of Na and Cl represents single Na^+ and Cl^- ions. We simulated three distinct systems, comprised of fullerenes, water, and 0.01, 0.1, and 0.4 M concentrations of electrolytes using CGMD.

Experimental studies have shown that the fullerene agglomeration mechanism changes from slow RLCA to fast DLCA with increase of NaCl salt concentrations [1,2]. For a dilute system with fullerene mass fraction of 0.001%, the critical salt concentration at which the transition occurs, was measured as ~ 0.1 M. To compare the effect of electrolyte concentration on fullerene agglomeration at high fullerene concentrations with that observed for dilute solutions (i.e., low fullerene concentrations) in the experimental studies, a range of concentration of electrolytes were simulated. However, in CGMD simulations, it is not feasible to directly follow the experimentally observed distributions of fullerene clusters, where the average hydrodynamic radius of fullerene particles is large (~ 75 nm). Therefore, we simulated systems with an initial distribution of fullerene clusters, which qualitatively mimics that in the experimental studies, albeit at a reduced length scale as shown in Fig. 1. The initial configuration comprised 216 fullerene clusters of varying sizes that were distributed randomly in the simulated systems. The average cluster size corresponds to six fullerenes.

The cutoff distance for nonbonded interactions for the CGMD simulations was 1.5 nm. In order to be consistent with the studies related to the CGMD model of fullerenes in water [81], a shift function was applied for electrostatic interaction from 0 nm and for Lennard-Jones (LJ) interactions from 0.9 nm. We performed an equilibration run (300 ps) until the total energy of each system reached a minimal value followed by a NVT production run for at least 50 ns. We used a stochastic velocity rescaling thermostat [83], with relaxation time 1 ps, to maintain constant temperature of 310 K. The equations of motion were integrated with a time step of 0.02 ps as chosen in the studies pertinent to CGMD simulations of fullerenes in water [81]. The particle mesh Ewald (PME) [84] method was used to account for the long-range electrostatic interactions. All CGMD simulations were performed with the GROMACS software package (v4.6.1) [85].

The formation of fullerene agglomerates is a dynamic process, where sizes and shapes of clusters and the number

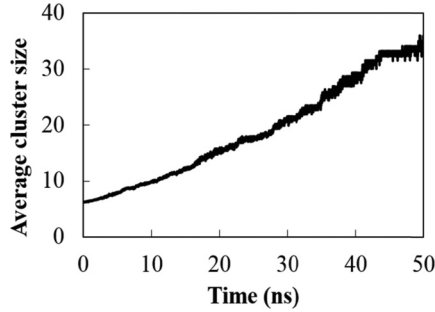


FIG. 2. Time evolution of the average fullerene cluster size, during CGMD simulation, is shown for a representative system with 0.1 M electrolyte concentration.

of neighbors of fullerenes in clusters change with time. Such change in cluster size causes the initial distribution of fullerene clusters to shift towards right with time when the agglomeration occurs irreversibly [2]. Figure 2 shows the evolution of the average size of fullerene clusters in the simulated system with 0.1 M salt concentration, chosen as a representative system. Although marginal dissociation occurs during the growth of fullerene agglomerates, it is evident from the figure that the association of fullerene clusters is the dominant process compared to dissociation. Moreover, the binding energy between fullerenes in water is ~ 15 kJ/mol $> k_B T$ [81]. Hence, it is unlikely for fullerene particles to dissociate after they aggregate. Therefore, we assumed irreversible aggregation of fullerene particles in our model, as done by numerous other studies [17,18,21,23,24,35]. We considered the initial 30 ns of production run of CGMD simulations to detect events. Since kMC is an event based method, it is important to obtain as many events as possible with corresponding rate constants to obtain statistically meaningful outcomes. Therefore, we made sure that during the sampled simulation time, we were able to capture sufficient number of events related to agglomeration of fullerene particles to calculate corresponding rate constants. Since the time interval between two consecutive frames in CGMD simulations was 0.02 ps, 30 ns production run generated 1.5 million frames, comprising the coordinates of the fullerene coarse-grained beads that were used for calculating rate constants of the events.

C. Defining events in CGMD simulations

The size of the fullerene particles, as well as the number of neighbors of individual fullerenes in the particles, changes due to agglomeration and can be assumed to be indicators of specific events. Therefore, we describe agglomeration events based on changes in the size of fullerene clusters and the number of neighbors of each fullerene in a cluster, which specifies the local environment of a given fullerene. In order to detect these events related to the agglomeration of fullerenes and calculate their rates, we developed an in-house code in C++. Our in-house code compared number of neighbors of individual fullerenes and the size of the cluster that contains it, between two consecutive frames. Specifically, the following steps were undertaken to determine events and corresponding rate constants.

(1) Each fullerene at every simulation time frame was mapped to the size of the cluster that contains it. Any mismatch of the cluster size between consecutive frames indicates that the fullerene cluster goes through an event. An event comprises growth of the cluster via collision and agglomeration with another cluster. In contrast, no change in the cluster size indicates either: (a) no fullerene agglomeration occurred; or (b) agglomeration and dissociation of identical number of fullerenes occurred simultaneously. Since the duration between consecutive simulation frames that were sampled was sufficiently small, we assumed that occurrence of concurrent agglomeration and dissociation in a cluster is not feasible.

(2) If any change in the size of a fullerene cluster was detected in step 1, we compared the number of neighbors of individual fullerenes in that cluster. Fullerenes were considered neighbors when their centers of mass (COM) distance was within 1.15 nm in the cluster. For any change in neighbors of the fullerenes, we checked whether the fullerenes and their new neighbors were part of a same cluster in the previous frame. If the fullerenes and the neighbors belonged to a same cluster in the consecutive frames, it indicates that a rearrangement of fullerene molecules occurred in the cluster. Such a rearrangement of molecules in a cluster was not considered as an event in our model. On the other hand, we conclude that an event occurred when the new neighbors of the fullerenes were found to be part of a different cluster in the previous frame. For convenience, we refer to such a fullerene as “seed fullerene” and such a neighbor as “added fullerene.” We denote the number of neighbors of the fullerene before the agglomeration as n_i . The number of neighbors of the fullerene that is added to the seed fullerene is designated as n_j and the size of the cluster that contains the added fullerene is designated as S .

Vectors comprising the three parameters (n_i, n_j, S) were used to define unique events in our model, where a seed cluster changed its state from A to B by agglomerating with an added cluster of size S . Here n_i was calculated based on the seed cluster and both n_j and S were calculated based on the added cluster. It should be noted that two separate events can be defined when any agglomeration event takes place, based on which of the two clusters is defined as the seed cluster. To illustrate this point, Fig. 3 presents schematics showing examples of events in the model. In the example, a cluster comprising three fullerenes, where each fullerene has two neighbors, and another cluster comprising two fullerenes, where each fullerene has one neighbor, agglomerate to form a cluster of size 5. According to our definition of events, two events occur from such a collision, where in event 1: $n_i = 2, n_j = 1, S = 2$ (top panel in Fig. 3), and in event 2: $n_i = 1, n_j = 2, S = 3$ (bottom panel in Fig. 3). That means event 1 occurs when the cluster comprising three fullerenes is considered as the seed cluster, while event 2 occurs when the seed cluster comprises two fullerenes.

D. Calculation of rate constants of events from CGMD simulations

Following the procedure mentioned above, all possible clustering events that occur in the CGMD simulations were captured. The transition rate constant k_{A-B} for an event was

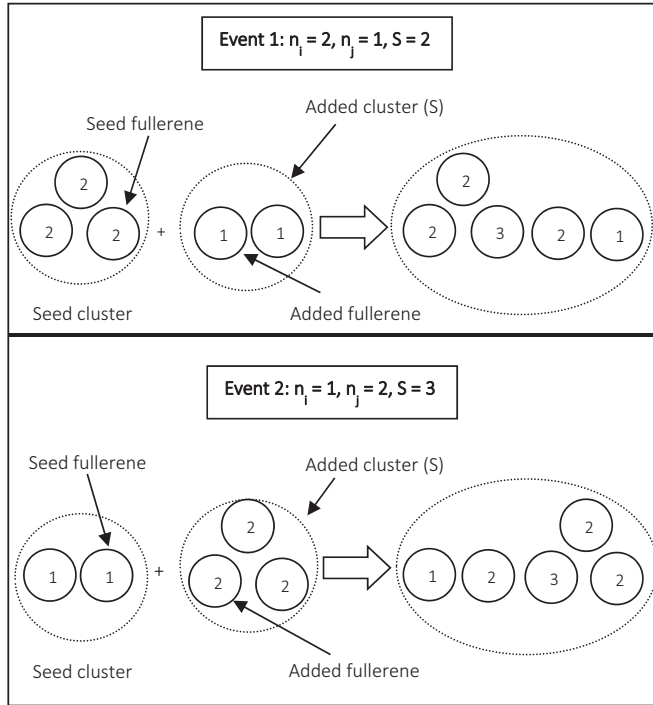


FIG. 3. The definition of events is illustrated pictorially using consecutive CGMD frames, with occurrence of an intermediate clustering event. Two examples of such events are shown in the top and bottom panels. Each circle represents a fullerene and the number inside the circle designates the number of neighbors of the fullerene. For convenience, each cluster is marked with dotted lines.

calculated using the following equation:

$$k_{A-B} = \frac{\sum_{m=1}^{m=TI} (e_{A-B})_m}{\Delta t_{MD} TI \left\{ \frac{\sum_{p=1}^{(f-1)} (n_i)_p}{(f-1)} \right\}}. \quad (5)$$

Here e_{A-B} is the number of occurrences of event A to B in 30 ns, Δt_{MD} is the time step (0.02 ps) for integration in the CGMD simulations, and f is the total number of frames (1.5 million) considered to calculate rate constants of the events. TI is the total number of intervals considered, which can be related to the number of frames as $TI = (f - 1)$. Piana *et al.* [73,74] used a very similar approach to calculate rate constants of events relevant to urea crystal growth. A table of the observed events defined above was created with corresponding rate constants k_{A-B} obtained by analyzing the CGMD trajectory. These rate constants were used for performing kMC simulations described below in detail.

E. Kinetic Monte Carlo simulations

As discussed earlier, a kMC trajectory consists of a sequence of discrete changes from one cluster size and shape to another. A random selection of what size and shape is next visited and the advancement of time after the occurrence of the corresponding change follow the probabilities prescribed by the master equation, Eq. (1), and Eqs. (2)–(4). The probability of transition from one state to another depends on the rate constants k_{A-B} obtained from Eq. (5). We used a standard

kMC approach to grow fullerene agglomerates using the rate constants obtained from the CGMD simulations.

According to our kMC model, a seed cluster undergoes changes in size and shape due to various agglomeration events. kMC is a stochastic process and each run provides distinct output. Therefore, sampling sufficiently large number of trajectories provides more accurate results. In an effort to obtain statistically reliable data, we performed at least 35 kMC runs for each system. Each kMC run consisted of 3000 steps, resulting in large fullerene clusters (size $\sim 30\,000$) and was sufficient to predict the growth mechanisms of the clusters in the simulated systems. In an effort to generate a meaningful initial seed cluster and pick clusters that need to be added to the seed cluster during kMC simulations, we recorded the configurations of all possible cluster sizes and shapes generated in the 30 ns run of the CGMD simulations and created a database of such clusters. We selected one of these clusters randomly as the initial seed cluster for each kMC run. Figure 4 shows the procedure that we followed to perform each kMC step. The diagram shows that we identified an event to occur at each kMC step following step 2 to step 6. After identifying the event, it was carried out at step 7. The time was updated at step 8 after the event occurred. Finally, we returned to step 2 to perform the next kMC step. We followed the following procedure at step 7 to carry out the event:

- First we obtained n_{ie} , n_{je} , and S_e for corresponding R_e from the event table.
- Then we searched for the fullerenes in the seed cluster that have n_{ie} neighbors. If multiple fullerenes had n_{ie} neighbors, we chose one of them randomly and called it “seed fullerene.”
- From the database of clusters we randomly selected a cluster of size S_e . The selected cluster was considered as the “added cluster” for the agglomeration.
- We searched for the fullerene, which had n_{je} neighbors, in the cluster chosen in (c). Again, if there was more than one fullerene, which had n_{je} neighbors, we selected one randomly and called it “added fullerene.”

(e) We placed the added cluster, chosen in (c), at a random position adjacent to the seed fullerene, chosen in (b), where the seed fullerene became the neighbor of the added fullerene, chosen in (d).

(f) Placing the added cluster randomly near the seed cluster might result in overlaps of fullerene molecules of the added cluster with that of the seed cluster. Since such overlaps are not physically realistic, we performed energy minimization on the final configuration of the cluster to remove overlaps. We used the steepest descent energy minimization module of Gromacs version 4.6.1 for this purpose. The procedures for removing overlaps performing energy minimization is discussed elsewhere [86–88].

For the sake of illustration of the kMC model, an example is shown in Fig. 5. In the example we have a seed cluster of size 4 from the cluster database. Following steps 2 to 7 in the above mentioned algorithm (Fig. 4) results in an event where $n_{ie} = 3$, $n_{je} = 1$, and $S_e = 2$. Figure 5 shows that there are two fullerenes in the seed cluster that have $n_{ie} = 3$. One of them (seed fullerene) is selected randomly and a cluster size of two (since $S_e = 2$) from the database are placed around the seed fullerene where the added fullerene has one

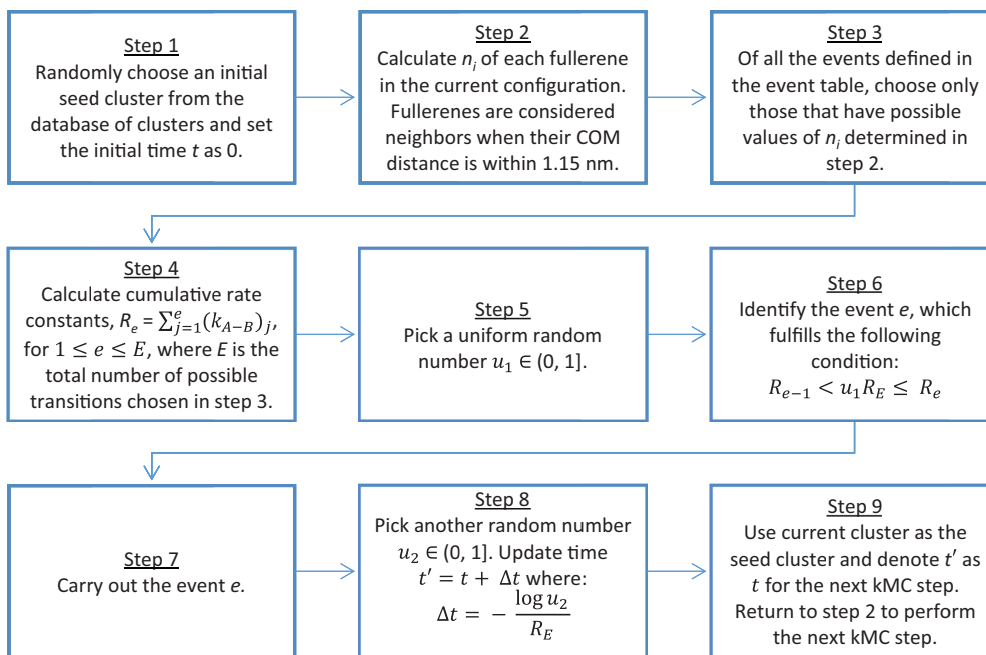


FIG. 4. (Color online) The procedure that was followed to perform each kMC step is shown. The arrows indicate the flow of the procedure.

neighbor (since $n_{je} = 1$) before the agglomeration. We make sure that after the agglomeration the seed fullerene and the added fullerene are neighbors. In the event that the fullerenes in the added cluster overlap with the fullerenes in the seed cluster, energy minimization is performed to remove overlap. This new configuration, after the agglomeration, becomes the initial configuration for the next kMC step. Identical procedure is followed in the next kMC step to generate another

new configuration. The cluster growth continues until the simulation is stopped after 3000 kMC steps.

As a simpler approach, we could have defined agglomeration events solely based on change in number of fullerenes in a cluster. However, such definition would not be able to select the specific fullerene site (according to our model, it is seed fullerene) in the seed cluster that collides and binds with the other fullerene site (according to our model, it is added fullerene) in the added cluster during the aggregation event. Losing this critical information would make the site of the aggregation reaction nonspecific. This would lead to arbitrary configurations of the subsequent aggregate thus making it impossible to track the shapes of aggregates. Additionally any definition of aggregation event based solely on size of participating cluster would limit the size of the cluster grown using kMC to the maximum cluster size observed in CGMD simulations. In contrast, the definition of clustering events that we employ in our model allows us to grow the fullerene cluster to sizes that are inaccessible to molecular simulations as well as track the shape of the growing cluster, thus making it versatile and applicable to a range of colloidal systems.

We emphasize that the kMC model considered implicit environment comprising electrolyte solutions, where fullerene clusters aggregated. In each kMC run, we tracked the growth of a seed cluster, which was surrounded by more than 150 million clusters obtained by analyzing the 1.5 million frames from CGMD simulations. The size distribution of the pool of fullerene clusters, used in kMC simulations for a representative system with 0.1 M electrolyte, is shown in Fig. 6. The cluster configurations that participate in an agglomeration event were not taken off from the system after the event. Therefore, the model system, in which the seed cluster grows, was assumed to be a grand canonical ensemble, where there was an unlimited supply of the fullerene clusters available to react with the seed cluster in each kMC step.

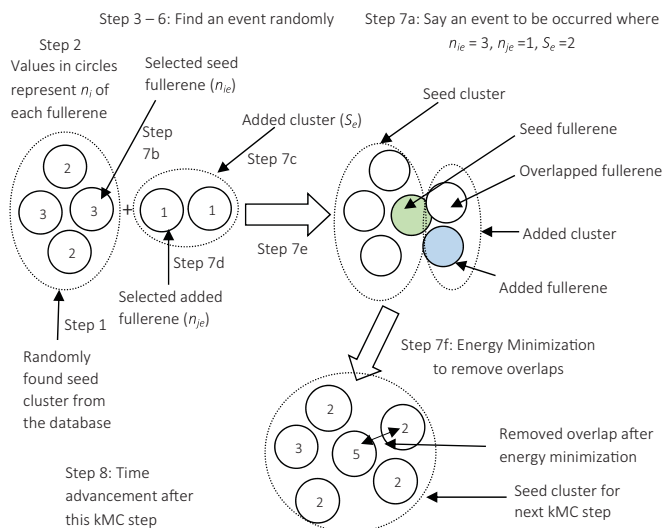


FIG. 5. (Color online) Formation of clusters of fullerenes utilizing the kMC model is shown as an example. Each circle represents a fullerene and the number inside the circle represents the number of neighbors of each fullerene in a cluster. For convenience, each cluster is marked with a dotted line. In this example, after the first kMC step, the cluster size increases from 4 to 6. The cluster growth continues until the simulation is stopped. The filled green circle (to the left of the overlapped fullerene) represents seed fullerene, while the filled blue circle (below the overlapped fullerene) represents added fullerene.

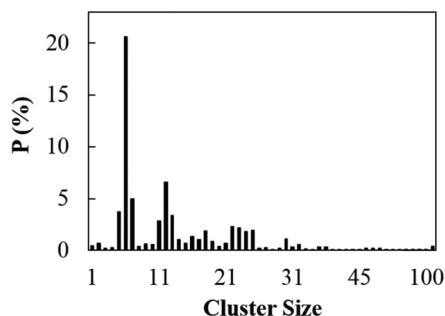


FIG. 6. Initial size distribution of clusters considered in kMC simulations of 0.1 M electrolyte solution, used as a representative system, is shown. Here P represents the relative occurrence of clusters of specific sizes in the simulated system, expressed as a percentage of the total number of clusters.

III. RESULTS AND DISCUSSION

Representative snapshots of a growing fullerene cluster in 0.1 M electrolyte solution, at distinct times during the kMC simulations, are presented in Fig. 7. In this particular representation, the initial seed cluster comprising 16 fullerenes, shown in Fig. 7(a), grows to a cluster of 181 fullerenes [Fig. 7(b)] after 20 kMC steps. During this process, the largest particle dimension increases from approximately 4 to 14.6 nm. After 60 kMC steps, the particle grows to a cluster of 710 fullerenes as shown in Fig. 7(c), where the largest dimension of the cluster is approximately 29 nm. The ensemble of fullerene clusters grown under identical conditions, represented by particles generated from multiple kMC runs after 3000 steps, each comprised more than 30 000 fullerenes and the average largest dimension was approximately 80 nm. In perspective, this dimension is 115 times the diameter of a single fullerene and inaccessible by the CGMD simulations alone simply considering the number of beads that would need to be simulated. The example therefore demonstrates that the model is able to grow fullerene clusters of significant size and could be possibly extended to other nanoparticles grown in other solvents. The objective of this particular study is to further demonstrate the CGMD-kMC model can predict the size and shape distribution of particles in solvents at time scales relevant to real-life applications in solvent-based processing of nanoparticles.

In order to determine the rate of growth of fullerene clusters as well as the clustering mechanism, we tracked the size and

shape of fullerene clusters as a function of time. The number of fullerenes in a cluster is designated as the cluster size (N) while the corresponding radius of gyration (R_g) is used as an indicator of the shape of the cluster. The cluster size and radius of gyration was determined at various salt concentrations to study the effect of electrolytes. As a first step, we compared the growth characteristics observed in CGMD and kMC simulations to show that the effect of salt concentration on the agglomeration of fullerene particles is qualitatively similar in both deterministic and stochastic frames. Next, we obtained a relationship between the cluster size and shape as a function of residence time to characterize the colloidal aggregation regime for the system. For the purpose of model validation, we compared the shape and size distribution of fullerene clusters predicted by our model with that reported by other modeling-based as well as experimental studies on fullerenes.

We obtained the change in average cluster size of fullerene with time from both CGMD and kMC simulations, shown in Fig. 8. In Fig. 8(a) we see that the average cluster size increases almost linearly with time in CGMD simulations. The initially dispersed fullerene particles diffuse in the simulated systems and stick to each other due to VDW attraction force. As mentioned in Sec. II, the short-range attractive force that causes the fullerenes to associate is very strong. Hence, we see in Fig. 8(a) that association of fullerene clusters is dominant compared to dissociation. Therefore, cluster size (N) increases with the advancement of time t . Figure 8(a) also shows that average cluster size at any given time is lower for systems with greater salt concentrations. For instance, the average cluster size is approximately 25 at 30 ns with 0.01 M salt concentration, while it is approximately 22 and 18 at salt concentrations of 0.1 and 0.4 M, respectively. This observation is not consistent with the previous studies [1,2,11] on fullerene agglomeration in electrolyte solutions, where the agglomeration rate increases with the increase of salt concentration. In general, the purpose of using salts in the solution is to reduce the electrostatic repulsion among clusters and enhance the sticking probability of particles. Hence, increasing salt concentration favors DLCA. However, such effects occur when the solution is very dilute, with the mass fraction of fullerene approximately at 0.001% [1,2,11]. In dilute solutions, the fullerene clusters are far apart and electrostatic repulsions stabilize the dispersion of the clusters. Hence, high salt concentration is required to screen the electrostatic repulsion completely and increase the aggregation

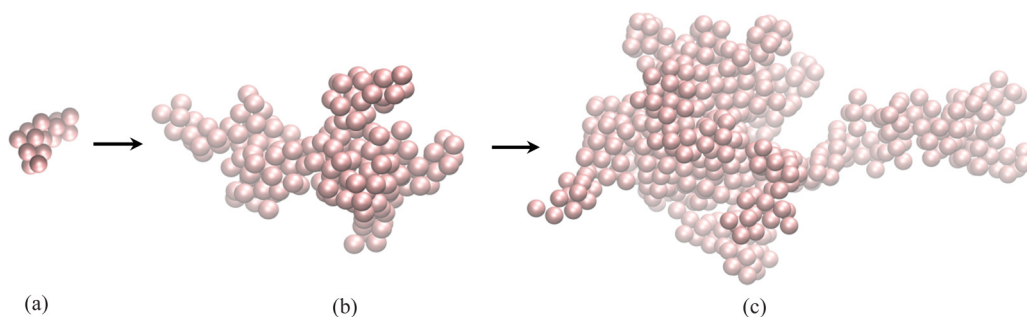


FIG. 7. (Color online) Representative clusters from a kMC run are shown to illustrate the growth of fullerene clusters. The initial seed cluster is shown in (a), where the cluster consists of 16 fullerenes. Using kMC simulation, the initial cluster was grown to a cluster consisting of (b) 181 fullerenes and (c) 710 fullerenes.

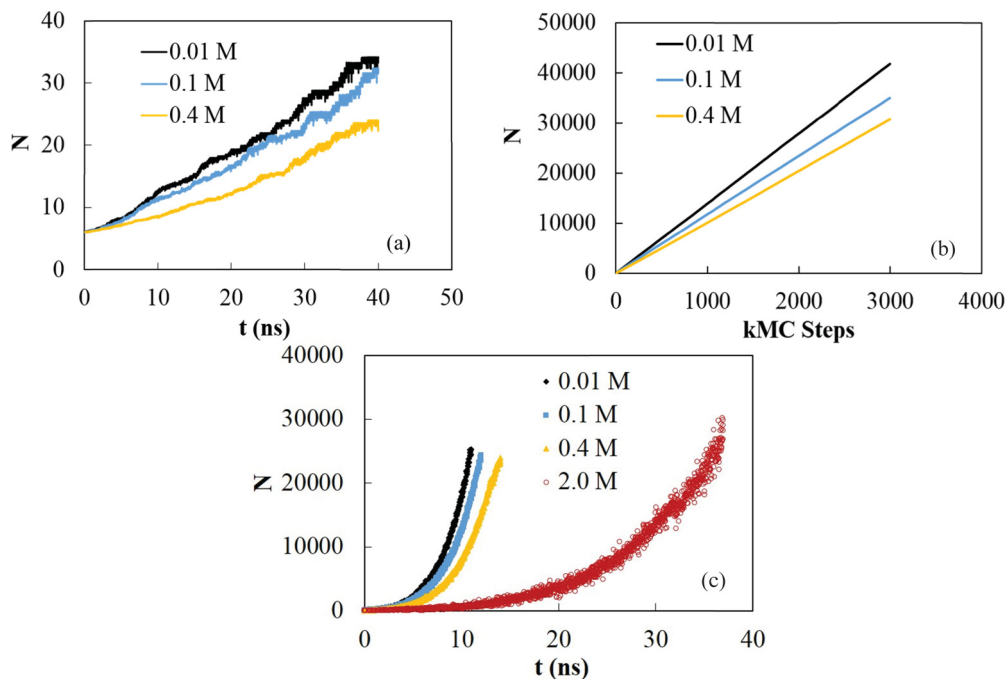


FIG. 8. (Color online) Average cluster size at various salt concentrations obtained from (a) CGMD and [(b) and (c)] KMC simulations are shown. Average cluster size with progressing kMC steps is shown in (b), while that at different times is shown in (c).

of fullerene nanoparticles. In contrast, our simulated systems comprised relatively high fullerene concentration, where the mass fraction of fullerene was approximately 7%. Due to such high fullerene concentration, VDW attractions among the clusters dominated over electrostatic repulsions and decreased the activation energy for the aggregation. Hence, the fullerene particles diffused randomly and aggregated to form clusters at a very low salt concentration (0.01 M). The high concentration of fullerenes in the systems with 0.1 and 0.4 M salt concentrations led to the formation of salt clusters that hindered the agglomeration of fullerene. Hence, increase of salt concentrations decreased the agglomeration rate of fullerene in the CGMD simulations.

It should be noted here that modeling systems with low concentration of fullerenes is necessary to observe transition from the RLCA to DLCA regime. However, the time required to observe transition from slow aggregation process in the RLCA regime to fast aggregation process in the DLCA regime is significantly high. Thus modeling such systems and finding rate constants of relevant events using CGMD is challenging. In that perspective, our current model is limited to systems with relatively fast aggregation kinetics, such as those with high nanoparticle concentrations. However, our model is effective in understanding sol-gel systems, where the nanoparticle agglomerates are already in the DLCA regime and agglomeration is faster compared to the RLCA regime.

While CGMD simulations modeled canonical ensembles and are limited to a maximum ensemble-averaged cluster size of ~ 25 , kMC simulations are able to access growth of fullerene particles to much greater sizes in electrolyte solutions. We determined the cluster size after each kMC step and calculated the average cluster size at distinct steps obtained from 35 kMC runs for each system. The average cluster size increases

almost linearly with kMC steps, shown in Fig. 8(b). Since the database of clusters that surround a growing cluster in kMC is predetermined from the CGMD simulations and has a specific size range, the rate of increase in the cluster size with kMC steps, averaged over multiple runs, is constant. This is particularly true if averaging is done over a significant number of kMC runs. Although Fig. 8(b) shows that the curves are perfectly linear, it should be noted that minor fluctuation is noticed for small ranges in kMC steps. Further details are shown in Fig. S1 in the Supplemental Material [89]. Comparison between Figs. 8(a) and 8(b) clearly shows that the kMC simulations are able to grow clusters that are at least three orders of magnitude larger compared to those seen in the CGMD simulations. The varied slopes seen in Fig. 8(b) for distinct salt concentrations illustrate the decrease of growth rate of fullerene clusters with the increase of salt concentrations. Qualitatively, the effect of salt concentration on the agglomeration behavior of fullerene is similar in kMC and CGMD simulations. However, Figs. 8(a) and 8(b) present cluster size as a function of physical time and kMC steps, respectively. For better comparison, a plot of cluster size obtained from kMC with advancement of physical time is shown later in Fig. 8(c). We used well-established force fields in CGMD simulations to observe agglomeration of fullerene. The qualitative similar trends seen in the results from kMC and CGMD provide us confidence on the accuracy of our kMC model. Henceforth, we will discuss the results obtained from kMC simulations, unless mentioned otherwise.

Figure 8(c) presents the growth of fullerene agglomerate with time. Since kMC is a stochastic algorithm, the advancement of time in each kMC step is random. As a result, the time advancements at the end of all kMC runs were not identical. However, all the runs advanced at least 11 ns after 3000

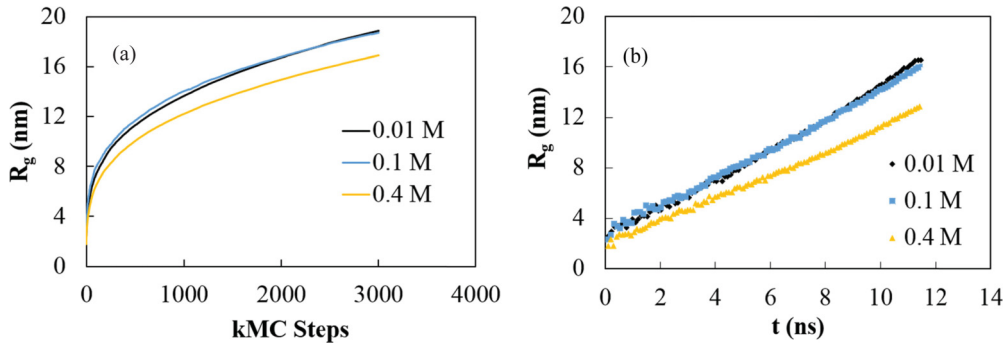


FIG. 9. (Color online) The evolution of the average radius of gyration at various salt concentrations with (a) kMC steps and (b) simulation time are shown.

kMC steps. Hence, the growth characteristics for different salt concentrations were plotted in Fig. 8(c) till 11 ns. However, it should be noted that the time advanced to approximately 18 ns after 3000 steps for the system with 0.4 M salt. Figure 8(c) shows that initially, when the cluster sizes were relatively small (comparable to that in CGMD simulations), the average cluster size increases linearly with time. The rate of increase of aggregate size $\frac{dN}{dt}$ at the initial stage is approximately 250/ns, while it is approximately 4000/ns at the final stage of the growth of clusters. It is evident that the number of interacting sites increases in a cluster with an increase in its size. It should also be noted that the aggregating cluster is surrounded by numerous fullerene particles and the probability of clustering of two particles is proportional to their number of available interacting surface sites [90]. Hence, an increasingly large number of interacting sites on the growing fullerene particle increases the growth rate in a nonlinear manner as the cluster size becomes significantly large. We will discuss the change in growth rate of fullerene clusters with time in more detail later. Figure 8(c) also shows that the fullerene agglomeration rate decreases with increase in salt concentration, which is consistent with the results presented in Fig. 8(a). We will later show that the fullerene aggregation mechanism is independent of salt concentrations for the simulated systems.

Although the time scale shown in the study is somewhat limited, our model is not restricted to such small time scales. For demonstration purposes, we simulated a system with the slow aggregation kinetics comprising 3.5% fullerenes by mass fraction and 2.0 M salt concentration. The growth of the particles in this particular system is represented with red circular markers in Fig. 8(c). The figure shows that the average cluster size in the system is $\sim 25\,000$ at ~ 38 ns. On the other hand, it requires less than 12 ns to observe the same average cluster size in the other systems. The rate of the events in these simulated systems are relatively large ($\sim 10^9/s$), since the fullerene concentration is high. It is noteworthy, however, that our model can access agglomeration processes that are too fast to be accessible to experimental studies.

To describe the shape of the growing cluster, we calculated the radius of gyration of each cluster both as a function of kMC steps and simulation time, shown in Figs. 9(a) and 9(b), respectively. The radius of gyration R_g of a fullerene cluster of size N is calculated using the equation $R_g(N) = \sqrt{\frac{1}{N} \sum_{i=1}^N [(x_i - x_{c.m.})^2 + (y_i - y_{c.m.})^2 + (z_i - z_{c.m.})^2]}$, where

i denotes distinct fullerenes, c.m. is the center of mass, and x , y , and z refer to position coordinates. It is observed that while N increases linearly with kMC steps, shown in Fig. 8(b), R_g follows the power function, presented in Fig. 9(a). Mathematically, the phenomenon can be interpreted in the light of well-established power law between cluster size N and R_g . Figure 9(a) shows that the slopes of the curves gradually decrease with the advancement of the kMC steps. For instance, R_g increases from approximately 2 to 6 nm in 50 kMC steps, while it increases from 6 to 10 nm in 300 kMC steps in the system with 0.1 M salt concentration indicating that the slope of the curve decreases nearly by a factor of 5 in the later steps. The decrease in the slope is significant as the kMC steps advance further. Similar phenomena are observed for other salt concentrations as well. A log-log plot (Fig. S2 in the Supplemental Material [89]) based on the data presented in Fig. 9(a) is nonlinear and indicates the transition of the dimensionality of the cluster with time. Based on the gradual reduction of the slopes of the curves in Fig. 9(a), we hypothesize that the shape of fullerene clusters is characterized by low dimensionality (either 1D or 2D) initially but transitions to higher dimensionality (3D) as the clusters grow with time. The authenticity of this hypothesis is investigated later in the light of the fractal dimension of the clusters. Figure 9(b) shows a linear relationship between the radius of gyration of clusters and simulation time at the initial stage. However, the curves slightly diverge from linearity when the cluster size N becomes significantly large and grows with time in a nonlinear manner as discussed earlier in connection with Fig. 8(c). The effect of salt concentration on the cluster size is remarkable, while its effect on the cluster shape is not very clear. However, one can crudely assume that the onset in the transition in dimensionality of clusters is delayed with the increase of salt concentration, since the agglomeration rate becomes slower.

In order to evaluate the dimensionality of fullerene agglomerates, we characterized the clusters by calculating their fractal dimension, since the aggregation process results in the formation of agglomerates with fractal shapes. The fractal dimension D_f can be obtained from the scaling relation between particle number N in a fullerene agglomerate and the radius of gyration R_g of that agglomerate $N \propto R_g^{D_f}$ [91]. We would like to emphasize that the fractal dimension of clusters is one of the most important quantities in describing cluster aggregation regimes, such as DLCA,

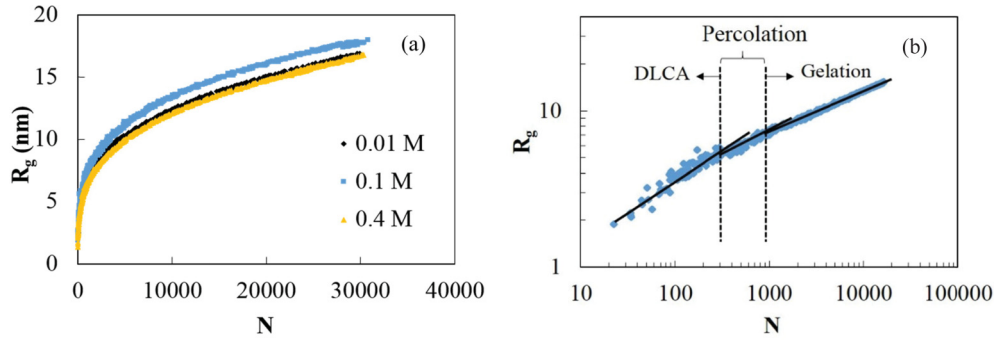


FIG. 10. (Color online) (a) Relationship between number of particles N in fullerene clusters and their radius of gyrations R_g during aggregation of fullerenes in the simulated systems are shown. (b) A log-log plot obtained from the R_g vs N curve for the system comprising 0.1 M salt is presented. The gradual change of the aggregation regime is demonstrated with the aid of three distinct fitted slopes at three size intervals.

RLCA, percolating cluster, and gelation. A majority of the previous studies on colloidal particle aggregation predicted fractal dimension of clusters to determine the shape of the clusters and the corresponding aggregation regime. Figure 10(a) shows that the radius of gyration and size of fullerene agglomerates follow the well-established power-law relationship [17–19,21,23,24,34,40,46,52,92]. The exponent of R_g , obtained from a curve fit, provides an estimate of the fractal dimension of the agglomerates. However, Fig. 10(a) and a representative log-log plot of R_g vs N [Fig. 10(b)] for 0.1 M salt concentration show a gradual change in slopes with an increase in size of fullerene clusters. The observed gradual change in the slopes from Fig. 10(b) suggests that a single fractal dimension does not characterize the structure of clusters formed and the aggregation regime during the growth. Hence, based on existing data in the literature and observation of cluster shapes from kMC runs, we have divided the plot into three distinct regions with different fitted slopes. The justification for the choice of three distinct regions is provided in detail later. The fitted slopes shown in Fig. 10(b) indicate the transitions of aggregation regimes and shapes during the growth of fullerene clusters. The data points in the three regions are plotted separately in Fig. S3 in the Supplemental Material [89] to illustrate the transition in more details. Identical trends are seen for other concentrations as well and are presented in Fig. 11 later.

The first region of Fig. 10(b) represents the size and shape of fullerene agglomerates at an initial stage. A linear fit with a goodness of fit $R^2 = 0.92$ indicates that the fractal dimension of the aggregates at the initial stage is approximately 1.9 (inverse of the exponent of N in the fitted curve). The obtained fractal dimension of the aggregates represents the DLCA regime. In this regime, the repulsive interactions among clusters are screened out and agglomeration of clusters occurs as soon as they collide, which is dominated solely by the diffusion of the clusters. The diffusion coefficient of fullerene particles has an inverse relationship with their size [93]. The initial distribution of the fullerene particles in kMC simulations indicates that the sizes of the clusters are small. Hence, at the beginning, the particles diffuse relatively fast, collide with each other, and stick when they are in proximity. The shape of clusters is ramified and hence the increase of R_g is relatively fast in the DLCA regime. The calculated fractal dimension of the clusters in this regime indicates that our statement about 2D shapes of the clusters based on the growth rate of R_g , shown in Fig. 9(a), is valid. Lin *et al.* [17] showed that the fractal dimensions of gold, silica, and polystyrene particles formed as a result of diffusion limited agglomeration are 1.86, 1.85, and 1.86, respectively. On the other hand, Liu *et al.* [53] demonstrated experimentally and numerically that the fractal dimension of diffusion limited fullerene agglomerates on a graphite substrate is ~ 1.9 . Meng *et al.* [2]

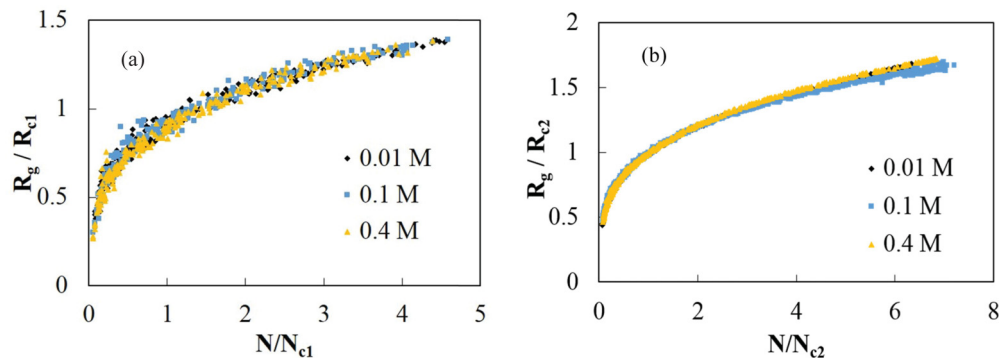


FIG. 11. (Color online) Normalizing N and R_g with the characteristic aggregation size N_c and radius of gyration R_c , determined for each salt concentration, results in superimposition of the curves obtained from the data presented in Fig. 10(a). The normalized plots are shown for (a) DLCA and percolating cluster aggregation regime and (b) percolating cluster and gelation regime.

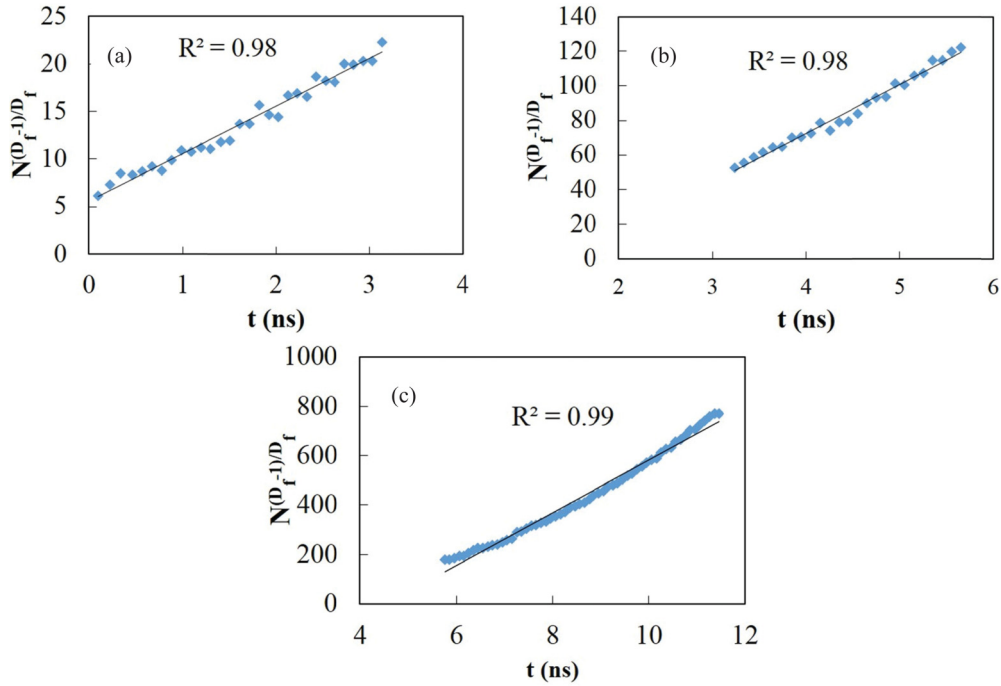


FIG. 12. (Color online) The relationship between N and t for (a) DLCA ($D_f \sim 1.9$), (b) percolating cluster ($D_f \sim 2.5$), and (c) gelation regimes ($D_f \sim 3.0$) in 0.1 M electrolyte solution are shown. The fitted slopes in the plots demonstrate the relationship $t \sim N^{(D_f-1)/D_f}$.

experimentally investigated the effect of salt concentration on the agglomeration behavior of fullerene particles in electrolyte solutions. Their results demonstrated fullerene aggregation through diffusion in a colloidal system with 0.001% fullerene concentration and 0.5 M NaCl salt. Although they mentioned that cluster shapes are open in nature at such conditions, the calculated fractal dimension of the agglomerates was ~ 2.05 , which suggests intermediate agglomeration between DLCA and RLCA regimes. However, based on the existing studies related to a colloidal DLCA process, it is evident that the fractal dimension of colloidal aggregates in DLCA regime is universal, which is 1.8 ± 0.1 [17,18,23,24,26], and our calculated fractal dimension of fullerene particles falls in the range.

Visualizing cluster shapes corresponding to sizes that span immediately beyond the DLCA regime indicates transition of shapes to less ramified structures within a narrow size range followed by nonramified structures. This observation of a continuous transition in the shapes of the agglomerates has been widely attributed to the phenomenon of continuous percolation reported in the scientific literature. In colloidal systems, continuous percolation is caused by increased connectivity between neighboring clusters. To account for this phenomenon, we fitted a straight line to the data corresponding to cluster sizes immediately greater than that for DLCA. The fractal dimension obtained from the data fit for this second region shown in Fig. 10(b) is determined to be approximately 2.5. This calculated value for fractal dimension is in good agreement with various studies, where irreversible DLCA aggregation of spherical colloidal particles was investigated [40,46,49–51,94]. The studies performed lattice and off-lattice Monte Carlo simulations and obtained clusters within the percolating cluster regime, where the fractal dimension of the particles is 2.5. As

mentioned before, the number of interacting sites increases rapidly with growth of the particles, which further leads to increase in aggregation rate that lead to nonlinear increase in size with time. At this stage, the fullerene particles are three dimensional and shapes of the particles are not ramified. According to the previous studies, such aggregates are called gels [40,42,50]. The data fit with $R^2 = 0.99$ in the third region of Fig. 10(b) indicates that the fractal dimension is approximately equal to 3.0. This indicates that the agglomerates in this regime form gel. Combining the results presented in Figs. 8(c) and 10(b) leads to the conclusion that the growth rate of clusters is 16 times faster in the gelation regime than in the DLCA regime. It is worthwhile to note that the fast growth rate in the gelation regime was observed in the above mentioned studies as well [40,46,49–51]. Overall, under the simulated conditions, the agglomeration process evolved from a DLCA regime to percolating clusters in transition and finally to the gelation regime. It should be noted that previous studies described the effect of electrolyte concentration on transitioning fullerene agglomeration from RLCA to DLCA regime at a certain fullerene concentration. In contrast, our study analyzed the evolution of cluster aggregation beyond DLCA regime and captures the fast dynamics of cluster aggregation during gel formation.

In order to establish the independence of salt concentrations on the agglomeration characteristics of fullerene clusters, as mentioned earlier, we normalized N and R_g , with a characteristic cluster size N_c and radius of gyration R_c at various salt concentrations. The values of N_c and R_c at various salt concentrations were estimated by finding the intersections of the slopes described in Fig. 10(b). We note that the technique of finding characteristic cluster size and radius of gyration was used in the studies pertinent to particle aggregation from

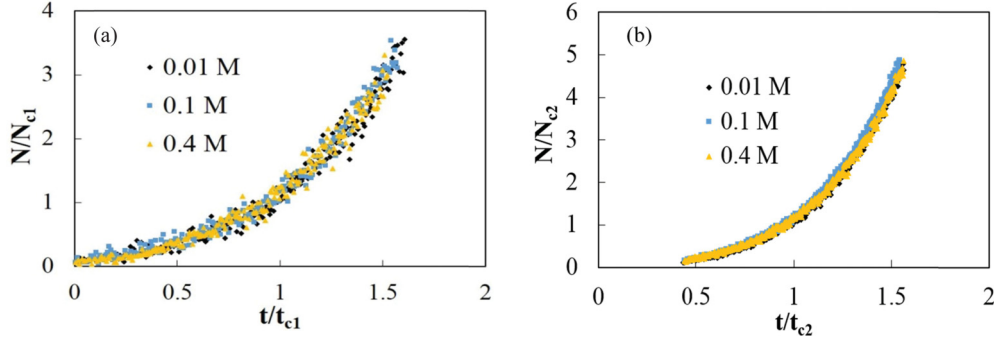


FIG. 13. (Color online) Normalizing N and t with the characteristic aggregation size N_c and time t_c , determined for each salt concentration, results in superimposition of the curves presented in Fig. 8(c). The normalized plots are shown for (a) the DLCA and percolating cluster aggregation regime and (b) percolating cluster and gelation regime.

DLCA regime to gelation regime mentioned earlier [40,46]. For convenience, we denote the intersection points of fitted slopes observed in the DLCA and percolating cluster regime, and in the percolating cluster and gelation regime, as 1 and 2, respectively. Hence, N_{c1} and R_{c1} are the characteristic cluster size and radius of gyration for first two regimes, while N_{c2} and R_{c2} represent the same for the latter two regimes. Normalizing N and R_g in the DLCA and percolating cluster regimes at various concentrations resulted in superimposition of the curves, shown in Fig. 11(a). The results indicate that on length scales less than R_{c1} , aggregates show a value of D_f corresponding to the DLCA process, while for length scales greater than R_{c1} , the value of D_f increases and correspond to percolation [40,46]. Similar superimposition was observed in percolating cluster and gelation regimes as well, shown in Fig. 11(b). Such superimpositions demonstrate that, in general, the transition of cluster aggregation regimes does not depend on salt concentration considered in the study. The results shown in Fig. 11(b) indicate that on length scales less than R_{c2} , the value of D_f indicates the presence of percolating clusters, while for length scales greater than R_{c2} , the value of D_f correspond to gelation of fullerene clusters. Overall, the results indicate that for $R_g < R_{c1}$, the shapes of the agglomerates are ramified in nature as obtained in DLCA regime and for $R_g > R_{c2}$ they are not ramified as obtained in the gelation regime.

In order to analyze the growth rate of fullerene clusters in various aggregation regimes, we have divided the plot, shown in Fig. 8(c), in three different regions based on the slopes. According to the study of Witten and Sander [34], the universal relationship between the growth rate of a cluster $\frac{dN}{dt}$ and its fractal dimension D_f is given by $\frac{dN}{dt} \sim N^{1/D_f}$. The solution to this equation gives $t \sim N^{(D_f-1)/D_f}$. In order to fit our simulation data to this universal form and determine D_f , we varied the exponents of N as $\frac{D_f-1}{D_f}$ in three distinct regions and plotted $N^{(D_f-1)/D_f}$ against time t . As a representative case, the system comprising 0.1 M salt was analyzed and results are shown in Fig. 12. The values of R^2 indicate good fit and effectively validate the results obtained from our aggregation model. While not shown here, we observed identical trends in the other simulated systems.

In order to generate a universal relationship between N and t , we normalized the cluster size and growth time with

N_c and t_c . The value of t_c was obtained from the intersection of the fitted slopes for the data presented in Fig. 8(c). For convenience we again denote the characteristic time for first two regimes as t_{c1} , while t_{c2} indicates the same for last two regimes. The superimpositions shown in Figs. 13(a) and 13(b) illustrate that the increase in $\frac{N}{N_c}$ is a universal function of $\frac{t}{t_c}$ and independent of salt concentration. Such a universal relationship was observed in the studies relevant to gel formation of spherical colloidal particles from the diffusion limited clusters mentioned above [46]. The studies showed that if the system starts from a DLCA regime and forms gel, the relationship between $\frac{N}{N_c}$ and $\frac{t}{t_c}$ is independent of the initial particle concentration. The results demonstrate that on time scales less than t_{c1} , the aggregates corresponded to the DLCA regime, while on time scales bigger than t_{c1} , the agglomerates referred to percolating clusters. Likewise, on time scales greater than t_{c2} , the aggregates indicated gel formation of fullerene clusters.

IV. CONCLUDING REMARKS

We have developed a model that utilizes CGMD and kMC to simulate the agglomeration of colloidal particles. The model was employed to study the growth of fullerene particles in electrolyte solution with varying salt concentration. The agglomeration events were defined based on changes in number of fullerenes in a cluster and local coordination environment of each fullerene in the cluster during agglomeration. The rate constants of a range of events were evaluated from CGMD simulations. The evaluated rate constants were employed in kMC simulations to grow fullerene agglomerates that range approximately from 1 to 100 nm. For a system with relatively high fullerene concentration (mass fraction $\sim 7\%$), both CGMD and kMC simulations separately indicated that the agglomeration rate of fullerene decreases with an increase of salt concentration. The results obtained from kMC simulations further indicate that the fullerene agglomeration mechanism is independent of salt concentration for these systems. The agglomeration process evolved from a DLCA regime to percolating clusters in transition and finally to a gelation regime. The fractal dimensions of the agglomerates obtained in DLCA ($D_f \sim 1.9$), percolating clusters ($D_f \sim 2.5$), and gelation

($D_f \sim 3.0$) regimes are in good agreement with that reported by other modeling based as well as experimental studies of colloidal systems. Master curves based on nondimensionalized cluster sizes and radii of gyration were obtained to characterize the transition of the agglomeration process. The characteristic radii of gyration R_{c1} and R_{c2} , and characteristic time t_{c1} and t_{c2} , were determined. The curves indicate that for $R_g < R_{c1}$ the shapes of the agglomerates are ramified in nature as obtained in a DLCA regime, while for $R_g > R_{c2}$ they are not ramified as obtained in a gelation regime. The characteristic time t_{c1} and t_{c2} describes the time required to reach the regimes.

We should note that combination of MD and kMC has been used in the past to analyze the growth of crystals in solutions, where the crystals grow on a predefined surface [73–75]. Due to the presence of the surface, the number of degrees of freedom as well as the number of events related to growth is relatively less. However, generic unrestricted growth of colloidal particles in solvents involves extremely complex dynamics and the number of clustering events is significantly large. Additionally, it is challenging to define the events in a manner that would enable modeling particle growth at a large length scale. To address this issue, in our model we tracked the change in local coordination environments of the particles during their growth. We have also used

the technique of energy minimization to remove overlap of the particles in kMC to obtain energetically meaningful intermediate structures. Our model is therefore able to access the growth of colloidal particles to much greater size in electrolyte solutions, while accounting for the atomistic interaction among particles. The model can also predict the agglomeration mechanism of colloidal particles, which is extremely important to control the shapes of clusters.

Overall, our model shows great promise and can be utilized in myriad applications, where agglomeration of colloidal particles is of interest. For instance, the agglomeration of nanosized colloidal particles in the presence of solvent and polymer can be characterized to predict the morphology of resulting thin nanocomposite films which find applications in the field of flexible electronics. The model can also be employed for investigating sintering processes that are increasingly being used in nanomanufacturing of components. Additionally, the model can be employed to study sol-gel processing of thin films for medical applications.

ACKNOWLEDGMENT

The authors gratefully acknowledge financial support from 3M Nontenured Faculty Grant program.

-
- [1] K. L. Chen and M. Elimelech, *Langmuir* **22**, 10994 (2006).
- [2] Z. Meng, S. M. Hashmi, and M. Elimelech, *J. Colloid Interface Sci.* **392**, 27 (2013).
- [3] A. R. Petosa, D. P. Jaisi, I. R. Quevedo, M. Elimelech, and N. Tufenkji, *Environ. Sci. Technol.* **44**, 6532 (2010).
- [4] C. Donini, D. N. Robinson, P. Colombo, F. Giordano, and N. A. Peppas, *Int. J. Pharmaceut.* **245**, 83 (2002).
- [5] X. Wang, J. Zhuang, Q. Peng, and Y. Li, *Langmuir* **22**, 7364 (2006).
- [6] N. I. Lebovka, *Polyelectrolyte Complexes in the Dispersed and Solid State I: Principles and Theory*, Advances in Polymer Science, Vol. 255 (Springer, New York, 2014), p. 57.
- [7] J. Y. Luo, J. Kim, and J. X. Huang, *Acc. Chem. Res.* **46**, 2225 (2013).
- [8] E. Y. Chi, S. Krishnan, T. W. Randolph, and J. F. Carpenter, *Pharmaceut. Res.* **20**, 1325 (2003).
- [9] L. K. Lee, C. N. Mount, and P. A. Shamlou, *Chem. Eng. Sci.* **56**, 3163 (2001).
- [10] J. Brant, H. Lecoanet, and M. R. Wiesner, *J. Nanoparticle Res.* **7**, 545 (2005).
- [11] K. L. Chen and M. Elimelech, *J. Colloid Interface Sci.* **309**, 126 (2007).
- [12] A. Tiraferri, K. L. Chen, R. Sethi, and M. Elimelech, *J. Colloid Interface Sci.* **324**, 71 (2008).
- [13] S. R. Chae, A. R. Badireddy, J. F. Budarz, S. H. Lin, Y. Xiao, M. Therezien, and M. R. Wiesner, *ACS Nano* **4**, 5011 (2010).
- [14] Y. Y. Yu, C. Y. Chen, and W. C. Chen, *Polymer* **44**, 593 (2003).
- [15] C. H. Yang, F. J. Liu, Y. P. Liu, and W. T. Liao, *J. Colloid Interface Sci.* **302**, 123 (2006).
- [16] L. P. Ravaro, D. I. dos Santos, and L. V. A. Scalvi, *J. Phys. Chem. Solids* **70**, 1312 (2009).
- [17] M. Y. Lin, H. M. Lindsay, D. A. Weitz, R. Klein, R. C. Ball, and P. Meakin, *J. Phys.: Condens. Matter* **2**, 3093 (1990).
- [18] P. Meakin, *Phys. Rev. Lett.* **51**, 1119 (1983).
- [19] P. Meakin and F. Family, *Phys. Rev. A* **38**, 2110 (1988).
- [20] T. A. Witten and P. Meakin, *Phys. Rev. B* **28**, 5632 (1983).
- [21] M. Kolb, R. Botet, and R. Jullien, *Phys. Rev. Lett.* **51**, 1123 (1983).
- [22] P. Dimon, S. K. Sinha, D. A. Weitz, C. R. Safinya, G. S. Smith, W. A. Varady, and H. M. Lindsay, *Phys. Rev. Lett.* **57**, 595 (1986).
- [23] D. A. Weitz and M. Oliveria, *Phys. Rev. Lett.* **52**, 1433 (1984).
- [24] D. A. Weitz, J. S. Huang, M. Y. Lin, and J. Sung, *Phys. Rev. Lett.* **54**, 1416 (1985).
- [25] Z. L. Zhang and S. C. Glotzer, *Nano Lett.* **4**, 1407 (2004).
- [26] D. W. Schaefer, J. E. Martin, P. Wiltzius, and D. S. Cannell, *Phys. Rev. Lett.* **52**, 2371 (1984).
- [27] C. Aubert and D. S. Cannell, *Phys. Rev. Lett.* **56**, 738 (1986).
- [28] G. Dietler, C. Aubert, D. S. Cannell, and P. Wiltzius, *Phys. Rev. Lett.* **57**, 3117 (1986).
- [29] G. Y. Onoda, *Phys. Rev. Lett.* **55**, 226 (1985).
- [30] J. M. Jin, K. Parbhakar, L. H. Dao, and K. H. Lee, *Phys. Rev. E* **54**, 997 (1996).
- [31] E. Dickinson, *Colloids Surf. B Biointerfaces* **20**, 197 (2001).
- [32] P. C. Hiemenz and R. Rajagopalan, *Principles of Colloid and Surface Chemistry*, 3rd ed. (Marcel Dekker, New York, 1997), p. 485.
- [33] Y. Xia, N. Trung Dac, M. Yang, B. Lee, A. Santos, P. Podsiadlo, Z. Tang, S. C. Glotzer, and N. A. Kotov, *Nat. Nanotechnol.* **6**, 580 (2011).
- [34] T. A. Witten and L. M. Sander, *Phys. Rev. B* **27**, 5686 (1983).
- [35] P. Meakin, *Phys. Scr.* **46**, 295 (1992).

- [36] M. Y. Lin, H. M. Lindsay, D. A. Weitz, R. C. Ball, R. Klein, and P. Meakin, *Phys. Rev. A* **41**, 2005 (1990).
- [37] B. J. Olivier and C. M. Sorensen, *J. Colloid Interface Sci.* **134**, 139 (1990).
- [38] F. Family, P. Meakin, and J. M. Deutch, *Phys. Rev. Lett.* **57**, 727 (1986).
- [39] S. Bastea, *Phys. Rev. Lett.* **96**, 028305 (2006).
- [40] S. D. Orrite, S. Stoll, and P. Schurtenberger, *Soft Matter* **1**, 364 (2005).
- [41] E. Dickinson, *J. Colloid Interface Sci.* **225**, 2 (2000).
- [42] L. L. Hench and J. K. West, *Chem. Rev.* **90**, 33 (1990).
- [43] P. J. Lu, E. Zaccarelli, F. Ciulla, A. B. Schofield, F. Sciortino, and D. A. Weitz, *Nature (London)* **453**, 499 (2008).
- [44] W. C. K. Poon, A. D. Pirie, and P. N. Pusey, *Faraday Discuss.* **101**, 65 (1995).
- [45] E. Dickinson, *Adv. Colloid Interface Sci.* **199**, 114 (2013).
- [46] M. Rottereau, J. C. Gimel, T. Nicolai, and D. Durand, *Eur. Phys. J. E* **15**, 133 (2004).
- [47] A. E. Gonzalez, G. Odriozola, and R. Leone, *Eur. Phys. J. E* **13**, 165 (2004).
- [48] A. Kapitulnik and G. Deutscher, *Phys. Rev. Lett.* **49**, 1444 (1982).
- [49] S. Babu, M. Rottereau, T. Nicolai, J. C. Gimel, and D. Durand, *Eur. Phys. J. E* **19**, 203 (2006).
- [50] J. C. Gimel, D. Durand, and T. Nicolai, *Phys. Rev. B* **51**, 11348 (1995).
- [51] J. C. Gimel, T. Nicolai, and D. Durand, *Eur. Phys. J. E* **5**, 415 (2001).
- [52] M. Y. Lin, H. M. Lindsay, D. A. Weitz, R. C. Ball, R. Klein, and P. Meakin, *Nature (London)* **339**, 360 (1989).
- [53] H. Liu, Z. Lin, L. V. Zhigilei, and P. Reinke, *J. Phys. Chem. C* **112**, 4687 (2008).
- [54] B. R. Saunders and M. L. Turner, *Adv. Colloid Interface Sci.* **138**, 1 (2008).
- [55] H. Hoppe, M. Niggemann, C. Winder, J. Kraut, R. Hiesgen, A. Hinsch, D. Meissner, and N. S. Sariciftci, *Adv. Funct. Mater.* **14**, 1005 (2004).
- [56] H. Hoppe and N. S. Sariciftci, *J. Mater. Chem.* **16**, 45 (2006).
- [57] T. Martens *et al.*, *Synth. Metals* **138**, 243 (2003).
- [58] J. Liu, Y. J. Shi, and Y. Yang, *Adv. Funct. Mater.* **11**, 420 (2001).
- [59] G. Brusatin and P. Innocenzi, *J. Sol-Gel Sci. Technol.* **22**, 189 (2001).
- [60] R. G. Alargova, S. Deguchi, and K. Tsujii, *J. Am. Chem. Soc.* **123**, 10460 (2001).
- [61] S. M. Mortuza and S. Banerjee, *J. Chem. Phys.* **137**, 244308 (2012).
- [62] F. Frigerio, M. Casalegno, C. Carbonera, T. Nicolini, S. V. Meille, and G. Raos, *J. Mater. Chem.* **22**, 5434 (2012).
- [63] S. Banerjee, *J. Chem. Phys.* **138**, 044318 (2013).
- [64] H. S. Marsh and A. Jayaraman, *J. Polymer Sci. Part B Polymer Phys.* **51**, 64 (2013).
- [65] E. Jankowski, H. S. Marsh, and A. Jayaraman, *Macromolecules* **46**, 5775 (2013).
- [66] R. C. Pani, B. D. Bond, G. Krishnan, and Y. G. Yingling, *Soft Matter* **9**, 10048 (2013).
- [67] N. R. Tummala, S. Mehraeen, Y.-T. Fu, C. Risko, and J.-L. Bredas, *Adv. Funct. Mater.* **23**, 5800 (2013).
- [68] N. G. Van Kampen, *Stochastic Processes in Physics and Chemistry*, 3rd ed. (Elsevier, New York, 2007), p. 1.
- [69] A. F. Voter, *Radiation Effects in Solids* (Springer, Netherlands, 2007), p. 1.
- [70] K. Reuter and M. Scheffler, *Phys. Rev. B* **73**, 045433 (2006).
- [71] A. P. J. Jansen, *An Introduction to Kinetic Monte Carlo Simulations of Surface Reactions*, Lecture Notes in Physics, Vol. 856 (Springer, Berlin, 2012), pp.1–254.
- [72] K. A. Fichthorn and W. H. Weinberg, *J. Chem. Phys.* **95**, 1090 (1991).
- [73] S. Piana and J. D. Gale, *J. Am. Chem. Soc.* **127**, 1975 (2005).
- [74] S. Piana, M. Reyhani, and J. D. Gale, *Nature (London)* **438**, 70 (2005).
- [75] A. M. Reilly and H. Briesen, *J. Chem. Phys.* **136**, 034704 (2012).
- [76] A. F. Voter and J. D. Doll, *J. Chem. Phys.* **82**, 80 (1985).
- [77] D. Konwar, V. J. Bhute, and A. Chatterjee, *J. Chem. Phys.* **135**, 174103 (2011).
- [78] A. F. Voter, F. Montalenti, and T. C. Germann, *Annu. Rev. Mater. Res.* **32**, 321 (2002).
- [79] R. J. Allen, D. Frenkel, and P. R. ten Wolde, *J. Chem. Phys.* **124**, 024102 (2006).
- [80] S. J. Marrink, H. J. Risselada, S. Yefimov, D. P. Tieleman, and A. H. de Vries, *J. Phys. Chem. B* **111**, 7812 (2007).
- [81] L. Monticelli, *J. Chem. Theory Comput.* **8**, 1370 (2012).
- [82] J. Wong-Ekkabut, S. Baoukina, W. Triampo, I. M. Tang, D. P. Tieleman, and L. Monticelli, *Nat. Nanotechnol.* **3**, 363 (2008).
- [83] G. Bussi, D. Donadio, and M. Parrinello, *J. Chem. Phys.* **126**, 014101 (2007).
- [84] T. Darden, D. York, and L. Pedersen, *J. Chem. Phys.* **98**, 10089 (1993).
- [85] B. Hess, C. Kutzner, D. van der Spoel, and E. Lindahl, *J. Chem. Theory Comput.* **4**, 435 (2008).
- [86] M. C. Payne, M. P. Teter, D. C. Allan, T. A. Arias, and J. D. Joannopoulos, *Rev. Mod. Phys.* **64**, 1045 (1992).
- [87] K. Zimmermann, *J. Comput. Chem.* **12**, 310 (1991).
- [88] R. S. Maier, J. B. Rosen, and G. L. Xue, *Proceedings of the 1992 ACM/IEEE Conference on Supercomputing, Minneapolis, MN* (IEEE Computer Society Press, Los Alamitos, CA, 1992), pp. 778–786.
- [89] See Supplemental Material at <http://link.aps.org/supplemental/10.1103/PhysRevE.92.013304> for details of the growth of clusters at small ranges in kMC steps, the log-log plot based on R_g vs kMC steps, and the fractal dimension of the agglomerates obtained from log-log plot of R_g vs N in various aggregation regimes.
- [90] D. Achlioptas, R. M. D'Souza, and J. Spencer, *Science* **323**, 1453 (2009).
- [91] M. Kerker, *The Scattering of Light and Other Electromagnetic Radiation* (Academic, New York, 1969).
- [92] R. M. Ziff and K. Fichthorn, *Phys. Rev. B* **34**, 2038 (1986).
- [93] R. M. Ziff, E. D. McGrady, and P. Meakin, *J. Chem. Phys.* **82**, 5269 (1985).
- [94] J. C. Gimel, T. Nicolai, and D. Durand, *J. Sol-Gel Sci. Technol.* **15**, 129 (1999).